Evolution of the derivative skewness for nonlinearly propagating waves

Brent O. Reichman,[a] Michael B. Muhlestein, Kent L. Gee, Tracianne B. Neilsen, and Derek C. Thomas

Department of Physics and Astronomy, Brigham Young University, N283 ESC, Provo, Utah 84602, USA

(Received 21 November 2014; revised 19 January 2016; accepted 29 February 2016; published online 28 March 2016)

The skewness of the first time derivative of a pressure waveform, or derivative skewness, has been used previously to describe the presence of shock-like content in jet and rocket noise. Despite its use, a quantitative understanding of derivative skewness values has been lacking. In this paper, the derivative skewness for nonlinearly propagating waves is investigated using analytical, numerical, and experimental methods. Analytical expressions for the derivative skewness of an initially sinusoidal plane wave are developed and, along with numerical data, are used to describe its behavior in the preshock, sawtooth, and old-age regions. Analyses of common measurement issues show that the derivative skewness is relatively sensitive to the effects of a smaller sampling rate, but less sensitive to the presence of additive noise. In addition, the derivative skewness of nonlinearly propagating noise is found to reach greater values over a shorter length scale relative to sinusoidal signals. A minimum sampling rate is recommended for sinusoidal signals to accurately estimate derivative skewness values up to five, which serves as an approximate threshold indicating significant shock formation. © *2016 Acoustical Society of America*. [http://dx.doi.org/10.1121/1.4944036]

[MDV] Pages: 1390–1403

I. INTRODUCTION

The importance of nonlinearity during propagation has been a topic of significant debate in the jet noise community because of its tie to the growth of acoustic shocks. Many have shown evidence of nonlinear propagation for full-scale experimental data,[1–4] while some have seen evidence of nonlinear effects in model-scale jets,[5–7] and others have not.[8] Because of the difficulty in quantifying nonlinearity associated with statistical phenomena, much research has gone into the development and usage of various measures to quantify the effects and strength of nonlinearity and the presence of acoustic shocks in different situations. These measures have been developed in the time domain, using both the pressure waveform[9–11] and its first time derivative,[12–15] and in the frequency domain using higher order spectral analysis.[2,16,17] Although these various measures have been used as qualitative indicators of nonlinearity, a quantitative understanding of the values obtained has been lacking. This paper provides quantitative insight into the meaning of skewness values of the first time derivative of the pressure waveform, using analytical, experimental, and numerical methods.

Skewness is a statistical measure of asymmetry present in a probability density function and has been used in a wide variety of fields from agriculture[18] to economics.[19] In fluid mechanics, the skewness of the streamwise derivative of both the temperature[20] and velocity[21,22] has been used to indicate an increase in vorticity in turbulent flows. The skewness of the first time derivative of the pressure waveform, i.e., derivative skewness, is a measure of the asymmetry present in the derivative values of the waveforms. The derivative skewness has been shown to be associated with the presence of acoustic shock waves[23] and has been used to investigate nonlinearity present in the propagation of jet and rocket noise.[24–26] However, despite the use of this metric, a physical understanding of the connections between derivative skewness values, nonlinear propagation, and acoustic shock growth has yet to be fully investigated.

There are some examples of investigations into derivative skewness values for well-understood cases. One example, by Shepherd *et al.*[10] used the Blackstock bridging function as a solution to the Burgers equation to predict values for various statistics, including derivative skewness, for nonlinearly propagating sine waves and their evolution into sawtooth waves. They found that derivative skewness values dramatically increase during the shock formation process, in contrast to the pressure skewness, which changes only after the formation of shocks. The derivative skewness in random noise compared to sinusoidal signals has also been experimentally investigated using a plane-wave tube.[27] The preliminary analysis suggested that, for noise, the derivative skewness increased more rapidly and reached greater values.

This paper follows a structure similar to that of Muhlestein *et al.*,[28] who have carried out an analytical and quantitative investigation of another time-domain metric, the average steepening factor (ASF). First, an analytical treatment of derivatives skewness is considered for the Earnshaw,[29] Fubini,[30] and Fay[31] solutions to the Burgers equation for initially sinusoidal signals. Included is an analysis of the effects of additive noise and sampling rate. Next, these analytical solutions are compared against those obtained using numerical propagation. Finally, numerical results are compared against experimental data from a plane-wave tube for both sinusoidal and random noise waveforms. All of these analyses combine

[a]Electronic mail: brent.reichman@gmail.com

 0001-4966/2016/139(3)/1390/14/$30.00

to give a quantitative understanding of derivative skewness values observed during the formation and eventual decay of shock waves in continuous waveforms.

II. DERIVATIVE SKEWNESS

A. Definition

The skewness of a random variable, y, denoted by $\mathrm{Sk}\{y\}$, is a normalization of the third central moment of the probability density function (PDF) of y and is a measure of asymmetry in a distribution. The skewness of the first time derivative of the pressure waveform is defined in terms of the expectation values, $E[]$, as

$$\mathrm{Sk}\left\{\frac{\partial p}{\partial \mathrm{t}}\right\} = \frac{\mathrm{E}\left[\left(\frac{\partial p}{\partial t}\right)^3\right]}{\mathrm{E}\left[\left(\frac{\partial p}{\partial \mathrm{t}}\right)^2\right]^{3/2}}. \tag{1}$$

Because of the cubic power in the numerator, large values of $\partial p/\partial t$ are emphasized in the skewness calculation. It has been suggested by McInerny[24] that the skewness of the first time derivative of the pressure waveform, or derivative skewness, may be used to characterize shocks in rocket noise, and it has subsequently been used with crackle in jet noise, as crackle has been associated with acoustic shocks.[12,32] These shocks have high positive derivative values and moderate negative derivative values, meaning that the pressure waveform's derivative skewness increases as shocks form during propagation. Shepherd *et al.*[10] predicted the evolution of the derivative skewness for an initially sinusoidal wave propagating without linear losses in the preshock region. Subsequently, Muhlestein and Gee[27] calculated the derivative skewness for waveforms measured in a plane-wave tube and found trends that agreed with those predicted by Shepherd *et al*. This paper treats the evolution of the derivative skewness for an initially sinusoidal signal using analytical methods and compares the results with those obtained using numerical calculations and plane-wave tube experiments.

B. Burgers equation

The Burgers equation models the propagation of a planar wave including thermoviscous losses and nonlinear effects. Following the notation of Blackstock *et al.*,[33] the Burgers equation is written as

$$\frac{\partial p}{\partial x} - \frac{\delta}{2c^2}\frac{\partial^2 p}{\partial \tau^2} = \frac{\beta}{\rho c^3} p \frac{\partial p}{\partial \tau}, \tag{2}$$

where p is the acoustic pressure, x is the distance from the source, δ is a constant associated with acoustic absorption by the propagation medium, c is small-signal sound speed, $\tau = t - x/c$ is the retarded time, β is the coefficient of nonlinearity, and ρ is the ambient density. The terms on the left-hand side in Eq. (2) represent the total change in pressure with x and the effect of thermoviscous absorption; the right-hand side corresponds to the changes in pressure due to quadratic nonlinear phenomena. When nonlinear effects are sufficiently strong, the absorptive term in Eq. (2) is negligible in comparison with the nonlinear term, resulting in the lossless Burgers equation,

$$\frac{\partial p}{\partial x} = \frac{\beta}{\rho c^3} p \frac{\partial p}{\partial \tau}. \tag{3}$$

Under certain assumptions, useful analytical approximations and solutions to the lossy and the lossless Burgers equation may be found which are valid in different regions. The three expressions considered in this paper are the Earnshaw,[29] Fubini,[30] and Fay[31] solutions. These solutions are useful for our purposes because analytical forms of the time derivatives and the derivative skewness can be found for each of these solutions.

C. Earnshaw solution

The method of characteristics may be used to directly solve the lossless Burgers equation, Eq. (3), implicitly. This solution, called the Earnshaw solution,[29] can be written as a parametric equation

$$\begin{aligned} P &= g(\phi), \\ \phi &= t + \sigma P, \end{aligned} \tag{4}$$

where P is the pressure normalized by some pressure amplitude p_0, ϕ is the Earnshaw phase variable, t is time, and σ is a normalized distance away from the source.[33] The normalized distance is measured relative to the lossless shock formation distance, $\bar{x}$, which is defined for initially sinusoidal signals as

$$\bar{x} = \frac{\rho c^3}{\beta \omega p_0}. \tag{5}$$

In Eq. (5), $\omega = 2\pi f$, with f being the frequency of the initial sinusoid, and p_0 is its initial amplitude. For the remainder of this paper, distance is represented by $\sigma = x/\bar{x}$. At $\sigma = 1$, $x = \bar{x}$, and a theoretically discontinuous shock has formed. The Earnshaw solution, which is valid for $\sigma < 1$, may be interpreted as distorting the times of arrival of the initial waveform, represented by the Earnshaw phase variable, but not modifying the pressure values, $g = g(\phi)$.

An analytical form of the derivative skewness may be found for the Earnshaw solution. For an initially sinusoidal signal, the time derivative of the Earnshaw solution is written in parametric form as

$$\left(t', \frac{\partial P}{\partial t}\right) = \left(t - \sigma \sin(t), \frac{\cos(t)}{1 - \sigma \cos(t)}\right), \tag{6}$$

where t' represents the retarded time of arrival and $\partial P/\partial t$ is the time derivative at the retarded time of arrival. The expectation value of the nth power of the time derivative is

$$E\left[(\partial P/\partial t)^n\right] = \frac{1}{2\pi}\int_0^{2\pi}\left(\frac{\partial P}{\partial t'}\right)^n dt', \tag{7}$$

where $t' = t - \sigma\sin(t)$ is a retarded time that accounts for the variation in sound speed with acoustic pressure. It follows that $dt' = dt(1 - \sigma\ \cos(t))$. Substituting these values in Eq. (7) gives

$$E\left[(\partial P/\partial t)^n\right] = \frac{1}{2\pi}\int_0^{2\pi} \frac{\cos^n(t)dt}{(1-\sigma\cos(t))^{n-1}}. \tag{8}$$

This integral can be evaluated for $n = 2$ and $n = 3$ to give the analytical form of the derivative skewness, written as

$$\mathrm{Sk}\{\partial P/\partial t\} = \frac{2(1-\sigma^2)^{3/2} + 3\sigma^2 - 2}{(1-\sigma^2)^{3/4}\left(1-\sqrt{1-\sigma^2}\right)^{3/2}}. \tag{9}$$

Because the Earnshaw solution assumes lossless propagation, Eq. (9) depends only on σ.

The expression for the Earnshaw solution-based derivative skewness results in useful approximations. For $\sigma \ll 1$, Eq. (9) may be approximated as

$$\mathrm{Sk}\{\partial P/\partial t\} \approx 3\sigma/\sqrt{2}, \tag{10}$$

indicating that the nonlinear function shown numerically by Shepherd *et al.*[10] and experimentally by Muhlestein and Gee[27] can be approximated for small σ using a linear fit.[41] As $\sigma \to 1$, Eq. (9) may be approximated as

$$\mathrm{Sk}\{\partial P/\partial t\} \approx (1-\sigma^2)^{-3/4}, \tag{11}$$

which yields approximate values of 3.47 at $\sigma = 0.9$ and 18.9 at $\sigma = 0.99$ and then continues to increase towards infinity as $\sigma \to 1$.

D. Fubini solution

While the Earnshaw solution is useful in certain circumstances, an explicit function is sometimes more convenient. This is especially true when constructing waveforms at specific time intervals, as is the case when discussing the effects of a finite sampling rate subsequently. One explicit solution to Eq. (3) is the well-known Fubini solution,[33] written as

$$P = \sum_{n=1}^{\infty} \frac{2}{n\sigma} J_n(n\sigma)\sin(nt). \tag{12}$$

Similarly to the Earnshaw solution, the Fubini solution is only valid for $\sigma < 1$. Using the results developed in Appendix A for the skewness of an arbitrary Fourier series, an analytical form of the derivative skewness for $\sigma < 1$ can be found using the Fubini solution. The time derivative of Eq. (12) is an infinite cosine series, written as

$$\frac{\partial P}{\partial t} = \sum_{n=1}^{\infty} \frac{2}{\sigma} J_n(n\sigma)\cos(nt), \tag{13}$$

which allows the use of Eq. (A28) from Appendix A,

$$\mathrm{Sk}\left\{\sum_n A_n\cos(nt)\right\} = \frac{3}{\sqrt{2}} \frac{\sum_{n=1}^{\infty}\sum_{m=1}^{\infty} A_n A_m A_{n+m}}{\left[\sum_{n=1}^{\infty} A_n^2\right]^{3/2}}. \tag{14}$$

Equation (13) can be substituted into Eq. (14) and the derivative skewness can be written as

$$\mathrm{Sk}\{\partial p/\partial t\} = \frac{3}{\sqrt{2}} \frac{\sum_{n=1}^{\infty}\sum_{m=1}^{\infty} J_n(n\sigma)J_m(m\sigma)J_{n+m}((n+m)\sigma)}{\left[\sum_{n=1}^{\infty} J_n^2(n\sigma)\right]^{3/2}}, \tag{15}$$

where $J_n(x)$ represents the nth Bessel Function of the first kind.

Despite its analytical form, one disadvantage of the Fubini solution is the inability to exactly express the derivative skewness of a theoretically discontinuous shock due to the infinite series. Figure 1 shows the derivative skewness of an initially sinusoidal waveform and the discrepancy between the values obtained using the Earnshaw and Fubini solutions, with the solid black line representing the Earnshaw solution and the remaining lines representing the Fubini solution for a varying number of terms included in the sum. The Earnshaw solution approaches infinity as $\sigma \to 1$, but bandwidth limitations in the Fubini solution limit the values seen. Thus, if a theoretically discontinuous shock has formed at $\sigma = 1$ but measurement realities limit the usable bandwidth to $10^2 \cdot f$ or $10^3 \cdot f$, the maximum derivative skewness values would be approximately 10 or 30, respectively.

E. Fay solution

For waveforms with very large amplitudes, the relative length scales of nonlinear effects are much smaller than thermoviscous absorption. For such waveforms traveling in the sawtooth regime of propagation, typically thought of as

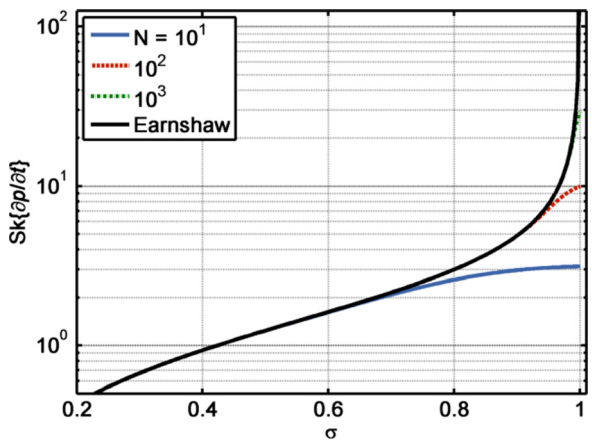

FIG. 1. (Color online) The analytical derivative skewness of an initially sinusoidal waveform modeled by the Earnshaw solution as a function of σ along with the estimated derivative skewness of the Fubini solution for N terms [see Eq. (12)].

$\sigma > 3$, another solution may be found. This solution is Fay's infinite series,[33]

$$P = \frac{2}{\Gamma}\sum_{n=1}^{\infty}\frac{\sin(nt)}{\sinh(n\psi)}, \tag{16}$$

where $\psi = (\sigma + 1)/\Gamma$, and Γ is the Goldberg 1 number, defined as $1/(\bar{x}\alpha)$, with α being the thermoviscous absorption coefficient at f_0. The Fay solution in Eq. (16) is valid for $\Gamma \gg 1$, signifying nonlinearity initially dominates thermoviscous losses. Similar to the Fubini solution, the time derivative of the Fay solution is a cosine series,

$$\frac{\partial P}{\partial t} = \frac{2}{\Gamma}\sum_{n=1}^{\infty}\frac{n\cos(nt)}{\sinh(n\psi)}. \tag{17}$$

From Eqs. (14) and (17), the derivative skewness of the Fay solution may be written as

$$\mathrm{Sk}\{\partial p/\partial t\} = \frac{3}{\sqrt{2}}\frac{\sum_{n=1}^{\infty}\sum_{m=1}^{\infty}\frac{n}{\sinh(n\psi)}\frac{m}{\sinh(m\psi)}\frac{n+m}{\sinh((n+m)\psi)}}{\left[\sum_{n=1}^{\infty}\frac{n^2}{\sinh^2(n\psi)}\right]^{3/2}}, \tag{18}$$

which depends, as expected, on ψ.

Figure 2 shows the derivative skewness of the Fay solution as a function of σ for different values of Γ. Though $N = 1000$ terms were used for all three values of Γ, the effect of including fewer terms is similar to that seen in Fig. 1 in that lower derivative skewness values are obtained for steepened or shock-containing waveforms. Because the effect of fewer terms has already been examined in Fig. 1, Fig. 2 instead includes multiple values of Γ. As expected, higher values of Γ have higher derivative skewness values, and lower values of Γ experience a large drop in derivative skewness values much sooner as they reach their respective old-age regimes, defined as $\sigma > \Gamma$. In the sawtooth region, for $3 < \sigma < \Gamma$, the derivative skewness drops as σ increases due to an increase in rise time in the shock, which is inversely proportional to the change in pressure over the shock.[33] It is interesting to note that a self-similar behavior is evident in the old-age regime for all three cases, as all three curves have derivative skewness values of $\sim$1.5 at $\sigma = \Gamma$ and similar slopes when plotted on a logarithmic scale.

F. Derivative skewness of acoustic shocks

As the waveform steepens and decays it enters and exits a region in which it is considered an acoustic shock. In most definitions of a shock, the rise time is used as the defining factor. Blackstock *et al.*[33] stated that a sinusoid remains in the sawtooth regime when the rise time, defined as the total time from the pressure minimum to the pressure maximum, is less than 20% of the period. This definition is useful but provides dissimilar results for the pre-shock and post-shock region, as the waveform shapes are significantly different. The pre-shock region contains rounded corners, while the post-shock region still maintains an N-wave shape. In an effort to accentuate the shortest rise times, Cleveland[34] and Loubeau *et al.*[35] defined rise time for impulsive signals as the time it takes for the pressure to rise from 10% to 90% of the maximum amplitude.

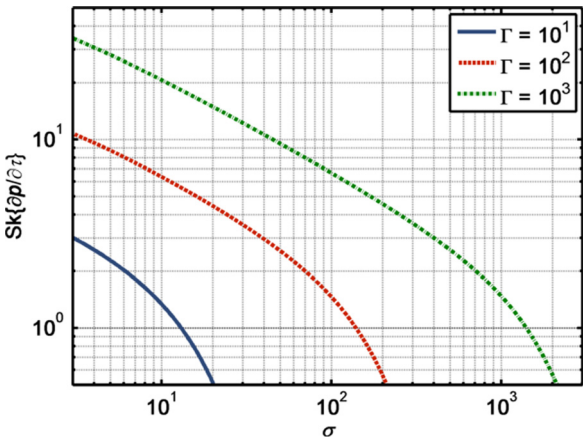

FIG. 2. (Color online) The derivative skewness of the Fay solution as a function of σ for three values of Goldberg number.

Because the impulsive signal definition lessens the difference between the pre and post-shock regimes, here we define a shock as occurring when the 10%–90% rise time is less than 5% of the period. Waveforms for the Fubini and Fay solutions that satisfy this definition of a shock are shown in Fig. 3 for a portion of the period T. The derivative skewness values of the solutions are 8.9 at $\sigma = 0.96$ and 3.9 at $\sigma = 260$, providing a range of values for which acoustic shocks begin to be significant. Derivative skewness values below this range likely indicate that the waveform does not contain shocks as defined, or that shock-like features are inadequately resolved due to sampling rate and noise limitations, as discussed in Sec. III.

III. MEASUREMENT CONSIDERATIONS

A. Finite sampling rate

Defining a shock based on the duration of the rise time lends itself to the question of the importance of sampling rate. If a shock is defined such that the rise time from 10%–90% is 5% of the waveform period, a sampling rate of 20 times the fundamental frequency must be used to guarantee even one point within the 5% window. However, this sampling rate is insufficient to capture the important difference in curvature between the waveforms shown in Fig. 3. The effects of discrete sampling on the estimate of the derivative skewness can be significant, since an inaccurate measure of the derivative may be accentuated by the cubic nature of the skewness.[36]

To investigate the inaccuracies associated with a finite sampling rate for the Fubini and Fay solutions, the effect of discrete sampling on the derivative of a general Fourier sine series is shown. The general results may then be applied to

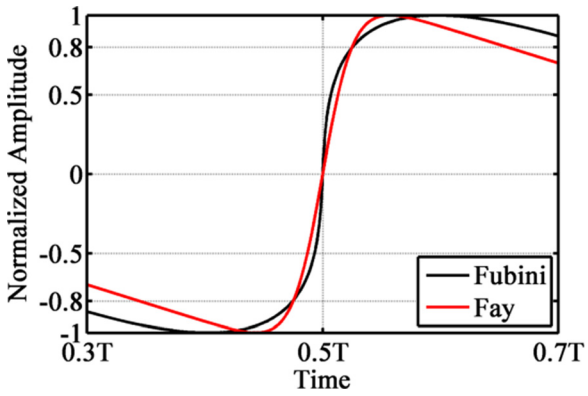

FIG. 3. (Color online) Shock profiles for normalized Fubini ($\sigma = 0.96$) and Fay ($\sigma = 260$, $\Gamma = 10^3$) solutions with derivative skewness values of 8.9 and 3.9, respectively, shown over a section of the period T. See text for shock definition.

the Fubini and Fay infinite series. If $f(t)$ is a Fourier sine series, written as

$$f(t) = \sum_{n=1}^{\infty} B_n \sin(nt), \tag{19}$$

an estimation of the first time-derivative of $f(t)$ can be obtained using a finite-difference technique. Here the series is written with B_n to be consistent with the Fubini and Fay solutions in Eqs. (12) and (16), respectively. The derivatives going forward will be approximated, both analytically and numerically, using a first-order, forward-difference approximation of the first derivative. Though it is possible that a higher-order method for approximating the first derivative could produce more accurate results, it should be noted that using a central differencing method artificially lowers derivative values across a coarsely sampled shock.[36] Using a constant time step, $\Delta t = f/f_s$, the derivative of Eq. (19) is approximated by

$$\frac{\Delta f}{\Delta t} = \frac{f(t+\Delta t) - f(t)}{\Delta t} \tag{20}$$

$$= \frac{1}{\Delta t}\sum_{n=1}^{\infty} B_n \sin(nt + n\Delta t) - \frac{1}{\Delta t}\sum_{n=1}^{\infty} B_n \sin(nt) \tag{21}$$

$$= \frac{1}{\Delta t}\sum_{n=1}^{\infty} B_n \big(\sin(nt + n\Delta t) - \sin(nt)\big). \tag{22}$$

Using the trigonometric identity $\sin(a+b) = \sin(a)\cos(b) + \cos(a)\sin(b)$, Eq. (22) becomes

$$\frac{\Delta f}{\Delta t} = \frac{1}{\Delta t}\sum_{n=1}^{\infty} B_n[\sin(nt)\cos(n\Delta t) + \cos(nt)\sin(n\Delta t) - \sin(nt)] \tag{23}$$

$$= \sum_{n=1}^{\infty} B_n \frac{\sin(n\Delta t)}{\Delta t}\cos(nt) + \sum_{n=1}^{\infty} B_n \frac{\cos(n\Delta t) - 1}{\Delta t}\sin(nt). \tag{24}$$

If we define

$$A'_n = B_n \frac{\sin(n\Delta t)}{\Delta t},$$
$$B'_n = B_n \frac{\cos(n\Delta t) - 1'}{\Delta t}, \tag{25}$$

then we may write Eq. (24) as

$$\frac{\Delta f}{\Delta t} = \sum_{n=1}^{\infty} A'_n \cos(nt) + \sum_{n=1}^{\infty} B'_n \sin(nt). \tag{26}$$

In the limit that $\Delta t \to 0$, we find that $A'_n \to nB_n$ and $B'_n \to 0$, which is the result obtained by assuming continuous sampling from the beginning. Thus, for a finite-sampled Fourier sine series, the first time derivative contains both sine and cosine terms. As this infinite sum involves both sine and cosine terms, we must use the skewness of a full Fourier series derived in Appendix A. Equation (26) is then used in conjunction with Eq. (A27) to estimate the derivative skewness for the Fubini and Fay solutions while taking into account a finite sampling rate.

1. Fubini solution

The effects of finite sampling rate for the Fubini solution are seen in Fig. 4 for various values of f_s/f, the sampling rate relative to the fundamental frequency. In Fig. 4(a) the derivative skewness of the discretely sampled Fubini solution is

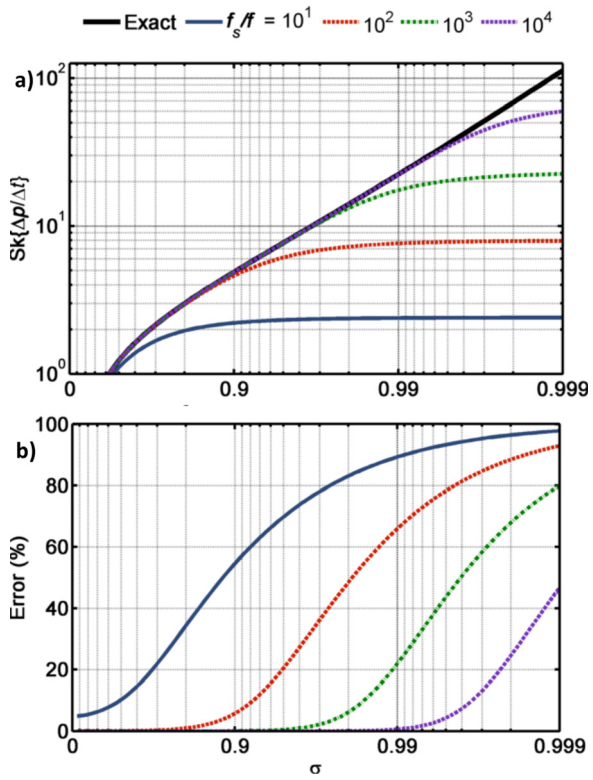

FIG. 4. (Color online) (a) Derivative skewness estimates of the Fubini solution for $f_s/f = 10^1$, 10^2, 10^3, and 10^4 along with the analytical Earnshaw calculation. For each curve, $f_s/2f$ terms were used to compute the estimates. (b) Error between the Fubini estimates and the Earnshaw solution.

plotted, while in Fig. 4(b) the error, relative to the continuously sampled Earnshaw solution, is shown. A limiting behavior is seen as a result of the finite sampling rate. Whereas the exact solution from Eq. (9) continues to increase on the logarithmic scale, going to infinity as $\sigma \to 1$, the discretely sampled derivative skewness estimates in Fig. 4 begin to approach respective maximum values. These values are less than the theoretical maximum for a given f_s/f (see Appendix B) because of the curved shock profile in the preshock region. For greater f_s/f, shorter rise times can be resolved, resulting in larger derivative skewness estimates. The divergent nature of the exact derivative skewness suggests that a derivative skewness estimate with any reasonable sampling rate ceases to approximate the actual value for σ sufficiently close to one. The point at which the discretely sampled estimate begins to underestimate the exact value depends on f_s/f. For example, the derivative skewness obtained using $f_s/f = 10$ diverges from the continuously sampled result above $\mathrm{Sk}\{\partial p/\partial t\} = 1$. When $f_s/f = 100$, an accurate estimate is obtained until $\mathrm{Sk}\{\partial p/\partial t\} = 5$, and for $f_s/f = 1000$ values of $\mathrm{Sk}\{\partial p/\partial t\}$ up to 12 can be accurately estimated.

2. Fay solution

The derivative skewness estimates of the Fay solution, shown in Fig. 5, show similar results to the derivative skewness estimates based on the Fubini solution. A limiting behavior is again dependent on the sampling rate relative to the fundamental frequency. However, as was discussed previously, the Fay solution has an N-wave shape and a more consistent slope than the Fubini solution, thus a lower sampling rate is required to achieve the same amount of accuracy. For example, for the $f_s/f = 100$ curve in Fig. 4, the derivative skewness begins to diverge at a value of 5, whereas in Fig. 5 the curve is accurate for derivative skewness values less than 7. As the wave enters the old-age regime, where $\sigma > \Gamma$, the shocks have decayed sufficiently that the derivative skewness values agree, even for very low relative sampling rates.

The effects of sampling rate have been identified in situations other than sinusoidal plane waves. Gee *et al.*[25] downsampled measured noise waveforms from an F-22 aircraft and found that by slightly decreasing sampling rate, derivative skewness values decreased accordingly. Insufficient sampling rate possibly explains relatively low derivative skewness values observed in laboratory-scale jet data despite the presence of acoustic shocks.[12,13]

3. Recommended sampling rates

Though a finite sampling rate will always underestimate a theoretically discontinuous shock, an adequate sampling rate may accurately calculate derivative skewness values to up to a certain threshold, so as to indicate shock formation. The Fubini solution is classified as containing a shock at $\sigma = 0.96$, with a corresponding derivative skewness values of 8.9. If this waveform is sampled at $f_s/f = 100$, there is a 28% error at this distance [see Fig. 4(b)]. The Fay waveform for $\Gamma = 1000$ decays to the point of no longer being a shock at $\sigma = 260$ with a derivative skewness of 3.9. At this point,

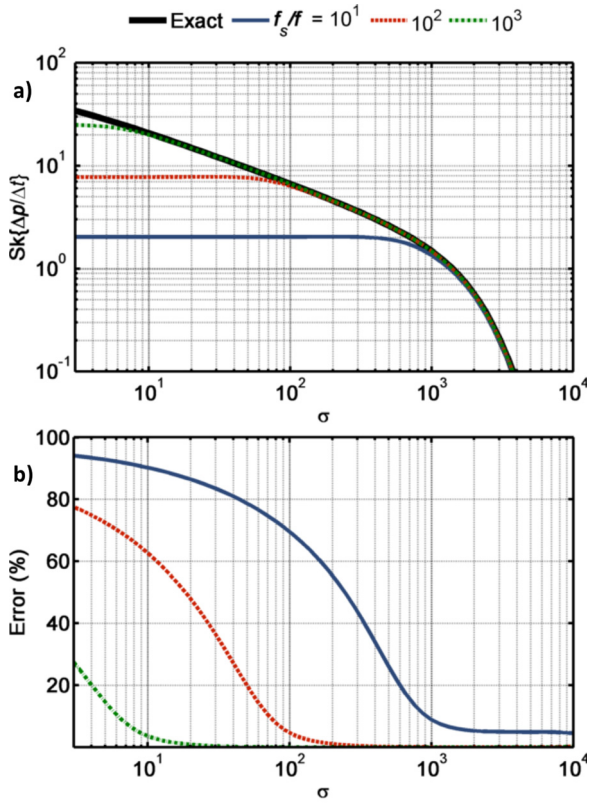

FIG. 5. (Color online) Estimates of the derivative skewness for the Fay solution as a function of σ and $f_s/f = 10^1$, 10^2, 10^3, and 10^4, with a Goldberg number of 1000. To calculate the estimates, $(f_s/f)/2$ terms were used. The exact derivative skewness derived from continuous sampling is plotted for comparison.

$f_s/f = 10$ underestimates the derivative skewness by nearly 50%, but $f_s/f = 100$ has negligible errors [see Fig. 5(b)]. Therefore, a minimum sampling rate of $f_s/f = 100$ is recommended to accurately estimate the derivative skewness during shock formation and decay. Using this sampling rate, derivative skewness values up to five will be accurately estimated for the sinusoidal case. Greater values, up to a theoretical maximum of 9.8, may be estimated using this sampling rate, but they may underestimate the actual shock steepness. Higher sampling rates provide additional shock detail and therefore accurate $\mathrm{Sk}\{\partial p/\partial t\}$ estimates for steeper shocks, but a minimum sampling rate of $f_s/f = 100$ is sufficient to obtain $\mathrm{Sk}\{\partial p/\partial t\} > 5$ as an approximate threshold for the presence of acoustic shocks in the waveform.

B. Signal-to-noise ratio

Additive noise can also impact derivative skewness values. Though such noise occurs in different ways, each with its own characteristics and statistics, investigation into the effects of additive, Gaussian noise on derivative skewness are illustrative of the robustness of this metric. Two cases are considered: first, the case of a steepened waveform in the pre-shock region at $\sigma = 0.75$, and second, a wave in the sawtooth region, at $\sigma = 30$ and $\Gamma = 1000$.

The waveforms are calculated at each distance using the Fubini and Fay solutions, respectively, following which bandpassed Gaussian noise is added to the waveform at various

signal-to-noise ratios (SNR), defined as $\mathrm{SNR} = 20\log_{10}(p_{\mathrm{rms}}/\mathrm{noise}_{\mathrm{rms}})$, where p_{rms} is the root-mean-square of the signal and $\mathrm{noise}_{\mathrm{rms}}$ is the root mean square of the noise. In order to avoid artifacts associated with filtering at a high sampling rate, a fourth-order Butterworth filter is used, with a center frequency of f_M and low and high cutoff frequencies of $f_L = f_M/1.41$ and $f_H = 1.41\, f_M$. Figure 6(a) displays the effect of additive noise for the steepened waveform at $\sigma = 0.75$, where the derivative skewness value of the original waveform is 2.51, for $f < f_M < 50f$, where f is the fundamental frequency of the sinusoid, and $0 < \mathrm{SNR} < 50\,\mathrm{dB}$. As would be expected, a higher SNR results in a derivative skewness calculation closer to the actual value. Additive noise introduces additional variations that mask the presence of the steepened waveform resulting in lower values of $\mathrm{Sk}\{\partial p/\partial t\}$. In addition, higher frequency noise has a greater effect than low-frequency noise on the accuracy of the derivative skewness. For $f_M = f$, a SNR of approximately 3 dB results in a measured value that is half the original derivative skewness. In contrast, the same reduction is seen at $f_M = 10f$ for $\mathrm{SNR} \cong 20\,\mathrm{dB}$. Higher frequency noise introduces larger amplitude derivative values, both positive and negative, than low-frequency noise of the same amplitude. These large-amplitude values are more likely to mask the larger derivative values of shocks in the expectation values used to calculate skewness. But because these expectation values are performed on a cubed quantity, the derivative skewness is likely to be less sensitive to the presence of additive noise than a metric such as the ASF,[28] where the linear average of $\partial p/\partial t$ is taken. In summary, care must be taken to maximize SNR when inspecting the derivative skewness of a waveform, as even small noise sources may artificially lower the derivative skewness values for high-frequency noise.

Figure 6(b) shows results similar to that of Fig. 6(a) but for a waveform in the sawtooth region at $\sigma = 30$. Because a shock is present in the waveform, the calculated derivative skewness is markedly higher, 12.23, and less likely to be masked in the derivative skewness by the presence of noise. In contrast with the Fubini solutions, at $f_M = 10f$ the presence of noise lowers the derivative skewness to half of the original value at $\mathrm{SNR} \cong 7.5$. Despite the resilience of the derivative skewness when shocks are present in the waveform, it is of note that high-frequency noise can still have a noticeable effect on calculated values, even with a high SNR.

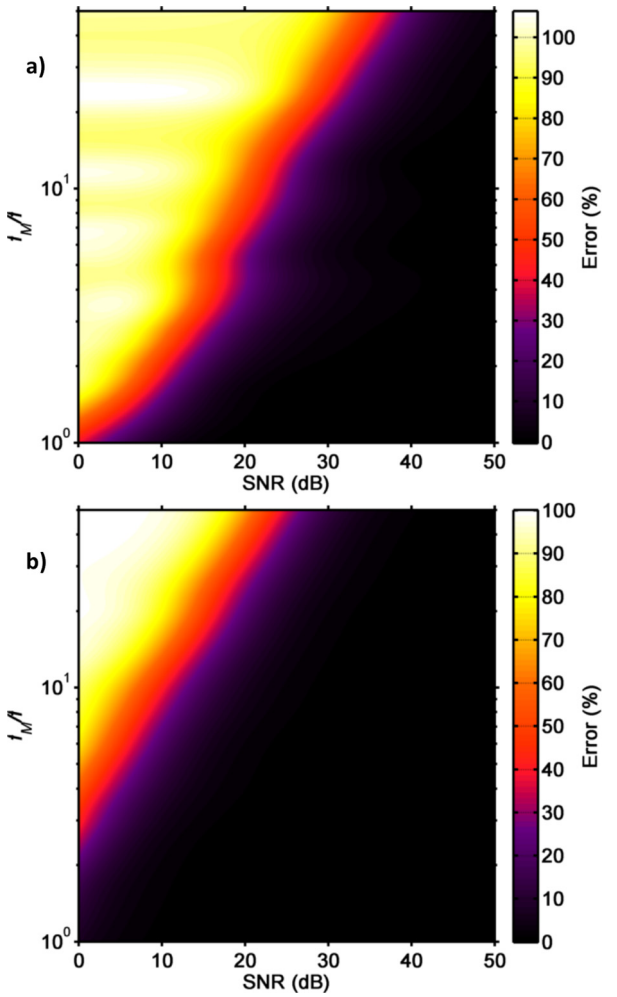

FIG. 6. (Color online) Derivative skewness error for an initial sinusoid propagated to a distance of (a) $\sigma = 0.75$ and (b) $\sigma = 30$ for $\Gamma = 1000$ with band-passed noise added to the signal at various SNR. The calculated derivative skewness with infinite SNR are (a) 2.51 and (b) 12.23.

IV. APPLICATIONS

A. Numerical case study

Though the above results give an understanding of the behavior of derivative skewness in the shock formation, sawtooth, and old-age regimes, it is useful to have a complete grasp of the trends observed throughout the entire process. In order to do this, $\mathrm{Sk}\{\partial p/\partial t\}$ for the spatial region between the preshock and sawtooth regimes must be calculated. Blackstock[37] presented a solution to the Burgers equation that served as a bridge between the Fubini and Fay solutions. By comparing amplitudes of the fundamental frequency as a function of σ he showed that for $\sigma > 3.6$, the difference between the "Blackstock bridging function" and the Fay solution was less than 2%.

Although an analytical representation of the derivative skewness of the Blackstock bridging function has not been found, the derivative skewness throughout the entire formation and decay of shock waves can be found using a numerical waveform propagation algorithm. The derivative skewness from the propagated waveform can be compared with the Earnshaw and Fay solutions in their regions of validity and give a complete view of $\mathrm{Sk}\{\partial p/\partial t\}$ during shock formation and decay. For the purposes of this paper, a propagation scheme based on the generalized Burgers equation[4] was used. Sinusoids with Goldberg numbers ranging from $\Gamma = 0.1$ to $\Gamma = 10^4$ are numerically propagated, and their derivative skewness is compared with results obtained using the analytical solutions described earlier. In order to provide a situation similar to experimental data considered later, a 1500 Hz initially sinusoidal waveform was sampled at 204 800 Hz, giving $f_s/f = 136.5$. This sampling rate suggests a maximum derivative skewness estimate of ~11.6 (see Appendix B) for the initially sinusoidal signal. The amplitude of the initial sinusoid was varied to correspond to values of Γ ranging from 0.1 to 10 000. Although the waveform has a fundamental frequency of 1500 Hz, due to the nondimensional nature of the analysis

and the assumption of thermoviscous absorption, the results show little variation with changing fundamental frequency for constant Γ and relative sampling rates.

The comparison of numerical and analytical derivative skewness values is shown in Fig. 7, with numerical predictions plotted as dashed lines and the analytical solutions plotted as solid lines. The Earnshaw solution is plotted for $\sigma < 1$ and the Fay for $\sigma > 3$. Values of Γ range from $10-^{1}$ to 10^{4}, but the Fay solution is not plotted for $\Gamma = 10^{-1}$ and 10^{0} because it is only valid for $\Gamma \gg 1$. The behavior seen using the numerical propagation of these waveforms conforms with expectations. A slight steepening of the waveform occurs, evidenced by the increase in derivative skewness, but the low initial waveform amplitude results in only minimal steepening, and absorption results in no shock formation. Both solutions diverge quickly from the Earnshaw solution as absorption dominates, but the curve for $\Gamma = 10^{0}$ reaches a much higher value than the curve for $\Gamma = 10^{-1}$. The curves for $\Gamma = 10^{1}$ and 10^{2} also show increased derivative skewness, with derivative skewness continuing to increase past $\sigma = 1$, peaking near $\sigma = \pi/2$, the theoretical location of the shock maximum amplitude. Differences seen between the numerical and analytical results are in large part due to two different effects. First, the Fay solution cannot be treated as exact for small values of σ or Γ. Second, slight error is introduced in the numerical propagation scheme due to the limited sampling rate and inability to fully characterize the acoustic shock. From past work,[34] it is recommended that 10^{-12} samples occur within the rise of the shock for numerical propagation, which is not achieved with the current sampling rate. The errors seen are very slight in the waveform itself, but slight changes in the waveform have a large impact on derivative values and thus $\mathrm{Sk}\{\partial p/\partial t\}$. Increasing the sampling rate by a factor of 10 dramatically improves results for $\Gamma = 10^{2}$. In Fig. 7, there is an error of 35.1% between the numerical and analytical solutions for the $\Gamma = 10^{2}$ curves at $\sigma = 3$. If the sampling rate is increased by a factor of 10, this error drops to 4.6%. The numerical absorption due to the limited sampling rate is different than the maximum derivative skewness value plateau that is seen for both the $\Gamma = 10^{3}$ and 10^{4} curves. The numerical and analytical curves for $\Gamma = 10^{3}$ both reach the maximum derivative skewness value defined by the sampling rate, but the numerical curve begins to decrease slightly before the analytical curve due to this numerical absorption. Though these issues are something that must be taken into account when numerically propagating shock-containing waveforms, the numerical propagation confirms the analytical results for both the Earnshaw and Fay solutions and serves as a bridge between them.

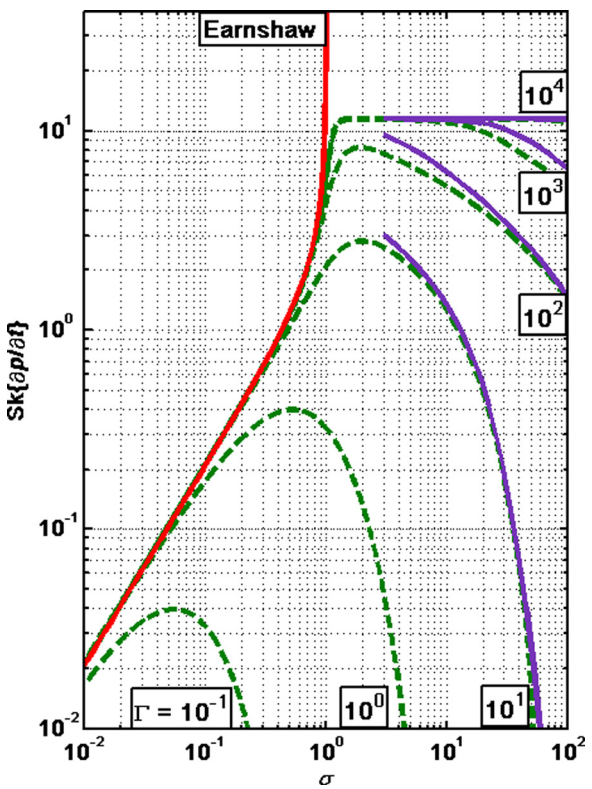

FIG. 7. (Color online) Derivative skewness of numerically propagated initial sinusoids with varying Goldberg numbers. The Earnshaw and Fay solutions are shown as solid lines, and the numerical predictions are shown in a dashed line.

As an example of the sensitivity of the derivative skewness to changes in the waveform, example analytical and numerical waveforms are presented in Fig. 8(a) for $\Gamma = 10^{2}$ and $\sigma = 3$. The waveforms themselves are very similar, but a very slight change in amplitude and a rounding of the edges of the shock is observed. These changes are more evident in Fig. 8(b), which shows the derivative of the waveforms in Fig. 8(a). The small changes in the waveforms result in larger changes in the derivative, which in turn has a large effect on the derivative skewness. The derivative skewness of the Fay solution shown is 9.53, while the numerically propagated signal has a derivative skewness of 6.18, giving an error of 35.1%. Because a small change in the waveform can have such a significant effect on derivative skewness, it is important that sampling rates be considered when numerically propagating shock-containing signals with the goal of calculating the derivative skewness.

B. Plane wave tube

1. Initially sinusoidal signal

In addition to numerical confirmation of the analytical results, the results have been also compared against experimental data. These data were obtained through use of a plane wave tube, constructed from sections of PVC pipe, each 3.05 m (10.0 ft) long with a 2.54 cm (1.0 in.) radius. A BMS 4590 coaxial compression driver was used to excite the tube and the tube was terminated anechoically with a wedge of fiberglass insulation. Five G.R.A.S. 40DD 3.18 mm (1/8 in.) microphones were mounted without gridcaps in holes drilled in the tube at distances of 0.4, 2.6, 5.6, 8.6, and 11.7 m from the driver. The microphones were flush mounted with the wall so they did not protrude and disturb the sound field. The driver was excited by a 1500 Hz signal such that the amplitude at the 0.4 m microphone was $p_0 = 547$ Pa, giving $p_{\mathrm{rms}} = 387$ Pa. This gives a lossless shock formation distance of 7.9 m, meaning that the farthest microphone is located at approximately $\sigma = 1.48$. The waveforms recorded were

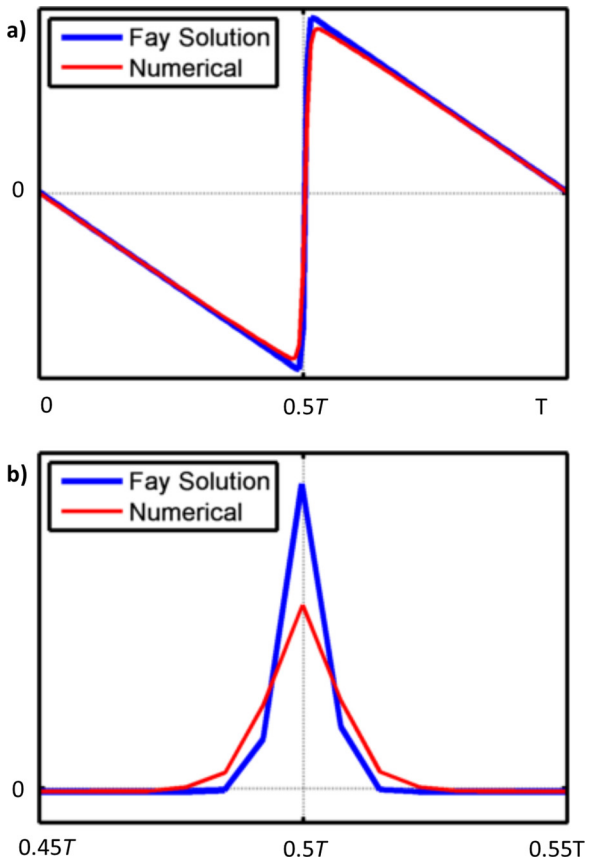

FIG. 8. (Color online) (a) Numerically propagated waveform compared with the Fay solution. (b) The derivatives of the waveforms in part (a). Small changes in the waveforms result in large derivative changes, which in turn result in large changes in the derivative skewness.

sampled at 204.8 kHz for approximately 6 s, giving $f_s/f = 136.5$, which puts the maximum derivative skewness for sawtooth waveforms at approximately 11.6. Derivative skewness values from the five waveform measurements have been calculated and compared with those predicted by numerically propagating the waveform measured at 0.4 m.

The waveforms from this experiment have been shown already by Muhlestein *et al.*[28] The figures in Ref. 28 show that the waveform steepens and forms a shock as it progresses down the tube. However, as shock waves form, a higher-frequency jitter can be observed in the waveforms, likely due to scattering of high harmonics by slight discontinuities at tube junctions. Nevertheless, the measured derivative skewness values agree well with estimates obtained through numerical propagation, as shown in Fig. 9. In the context of the SNR analysis above, the jitter is not of a sufficiently high frequency or amplitude to have a noticeable effect on the derivative skewness.

A similar comparison between the measured and numerical values has been completed in Ref. 28 for the ASF, which is the ratio of the average positive derivatives to negative derivatives in the waveform and the inverse of Gallagher and McLaughlin's wave steepening factor.[38] Since the ASF averages derivative values, the effect of one large derivative value is largely negated by the presence of many smaller values. On the other hand, the cubic nature of derivative skewness suggests that although $\mathrm{Sk}\{\partial p/\partial t\}$ can be affected by

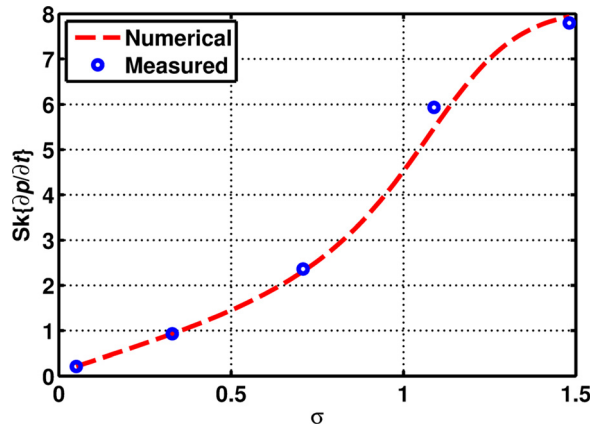

FIG. 9. (Color online) Comparison of derivative skewness values from measured waveforms in a plane wave tube with those of numerically propagated waveforms.

the presence of noise, its emphasis of large derivative values makes it less sensitive to noise than the ASF.

2. Broadband noise

Though the case of an initially sinusoidal wave provides significant physical insight, of broader interest is the propagation of noise. Although the different natures and PDFs of broadband noise and sinusoids prevent an immediate quantitative comparison of derivative skewness values, insights may still be gained by comparing trends. Because of the presence of larger outliers in noise, we expect noise signals to form shocks on a smaller length scale and reach greater derivative skewness values.[27] Using the same experimental setup as in the sinusoidal case, white noise was passed through a band-pass filter (700–2300 Hz) and propagated down the tube. Because of the broadband nature of the noise, the definition of $\bar{x}$ used earlier for sinusoids in Eq. (5) is no longer valid. Instead, we define a nonlinear distortion length similar to that of Gurbatov and Rudenko,[39]

$$\bar{x}_N = \frac{\rho c^3}{\beta(2\pi f_c)\left(\sqrt{2}p_{\mathrm{rms}}\right)}, \tag{27}$$

where f_c is the characteristic frequency of the noise. Here, the $\sqrt{2}$ is included so that as the noise bandwidth approaches zero, the sinusoid shock formation distance in Eq. (5) is recovered. In order to differentiate between the noise and sinusoidal cases, the normalized distance is now referred to as $\sigma_N = x/\bar{x}_N$.

As an example of broadband noise propagation, noise waveforms with $f_c = 1500$ Hz and $p_{\mathrm{rms}} = 286$ Pa at $x = 0.4$ m were measured. For this case, these input conditions yield $\bar{x}_N = 9.0$ m, a slightly greater distance than the shock formation distance of the sinusoidal signal. Figure 10 shows short waveform segments measured at 0.4 and 11.7 m, and the prediction made by numerically propagating the measured waveform at 0.4 to 11.7 m. In Fig. 10(b), a similar waveform jitter is present in the 11.7 m ($\sigma = 1.31$) waveform. However, by comparing Figs. 10(b) and 10(c), it can be seen that the

waveforms match well aside from the previously described jitter.

To more closely examine the spectral effects, Fig. 11 shows the power spectral densities associated with the three waveforms in Fig. 10. As the waveform propagates down the tube, wave steepening results in increases in level above the original cut-off frequency, and difference-frequency generation and possible wave coalescence increase the level below.[40] The spectra of the predicted and measured waveforms at 11.7 m are very similar, aside from the 10–35 kHz noise that is 30 dB down from the spectral peak and is the frequency-domain manifestation of the waveform jitter.

For the noise case, the waveform jitter is of sufficiently high frequency and amplitude to have a measureable difference in the derivative skewness. Figure 12 shows the measured and predicted derivative skewness values for waves of two initial amplitudes, the first with $p_{\mathrm{rms}} = 200$ Pa (140 dB re 20 μPa) and $p_{\mathrm{rms}} = 286$ Pa (143 dB re 20 μPa) for the second. These two cases in particular, were chosen because for all amplitudes of 200 Pa and below the ringing noise was present, but the SNR was great enough to have a minimal effect on derivative skewness, and for all amplitudes 286 Pa and above the ringing had a noticeable effect. There are a few features of note in Fig. 12. First, Sk$\{\partial p/\partial t\}$ reaches a higher value for the broadband noise than is possible in the sinusoidal case for the given sampling rate, as seen by comparing with Fig. 9. This corresponds with the initial experiment-based findings of Muhlestein *et al.*[28] Second, the derivative skewness has reached its highest value and is beginning to decrease by $\sigma_N = 1$, suggesting that the decay of shock waves is already occurring. This is likely because the definition used for $\bar{x}_N$ overestimates the actual distortion length.[27] Because broadband noise has a different PDF than sinusoidal noise, there are more outliers in terms of pressure, which are then more likely to form shocks earlier in the propagation than a sinusoid. Third, the ASF is steadily increasing throughout this range of σ, indicating that wave steepening is an ongoing process, even though the derivative skewness is decreasing. The largest shocks have already formed and started to decay, but the wave as a whole is still becoming more steepened. Fourth, for the higher amplitude case the measured derivative skewness values are markedly lower than predicted for higher values of σ_N, when shocks are likely well formed. This lower value is due to the presence of high-frequency jitter, as in the case of the sinusoidal signal. However, because the jitter is of a sufficiently high frequency and amplitude for the 286 Pa case, it creates a noticeable difference between the predicted and measured

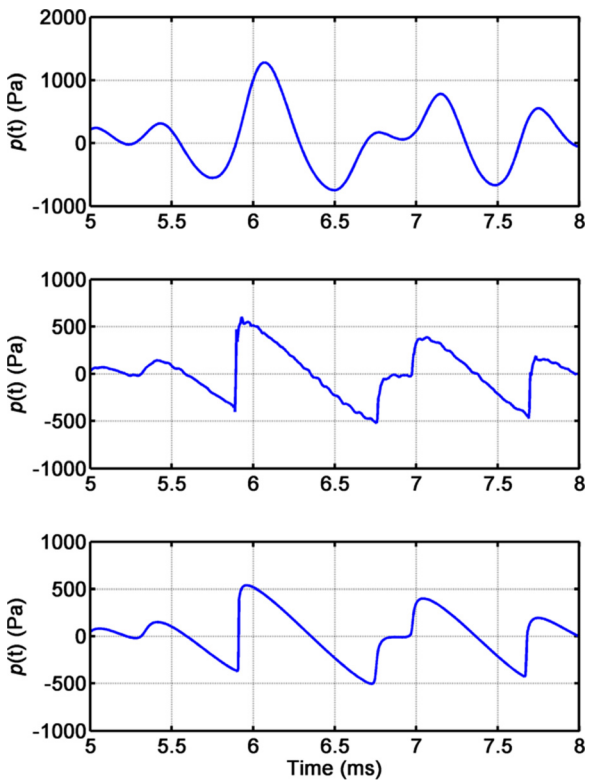

FIG. 10. (Color online) Measured noise waveforms at (a) 0.4 and (b) 11.7 m, and (c) the numerically predicted waveform at 11.7 m.

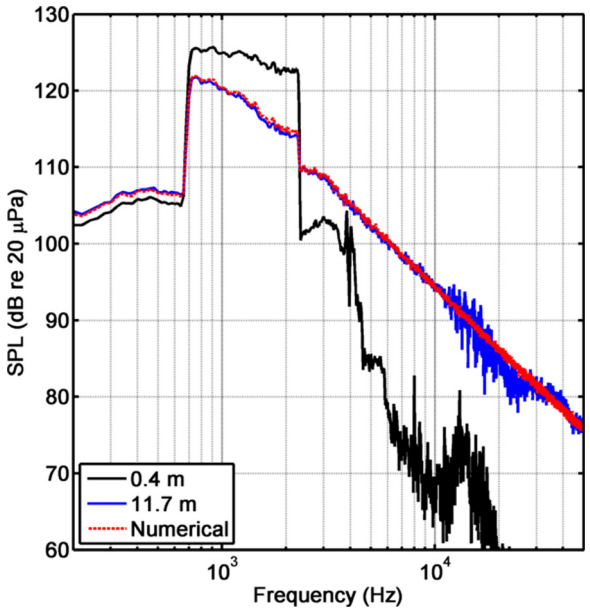

FIG. 11. (Color online) Spectra calculated from the three waveforms, segments of which were shown in Fig. 10. In the 11.7 m measured spectrum, high-frequency noise is present from 10 to 35 kHz.

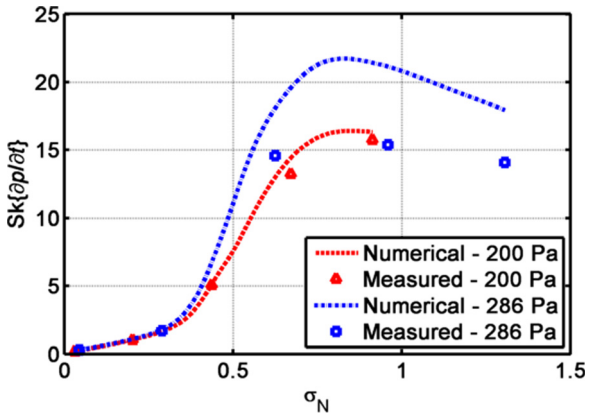

FIG. 12. (Color online) Predicted (dashed) and measured (dots) values of the derivative skewness as a function of $\sigma_N = x/\bar{x}_N$. Values shown are for $p_{\mathrm{rms}} = 286$ and 200 Pa. Both cases share similar growth initially, then different behavior with increasing σ.

TABLE I. The number of shocks present in two waveforms of different amplitudes, calculated from the waveforms measured at each of the five microphones. For this table a shock has been defined as a derivative exceeding 20 standard deviations of the waveform derivative.

	Mic locations	0.4 m	2.6 m	5.6 m	8.6 m	11.7 m
200 Pa	σ_N	0.031	0.203	0.437	0.671	0.913
	Derivative skewness	0.17	1.01	5.05	13.2	15.7
	Number of shocks	0	0	61	305	452
286 Pa	σ_N	0.045	0.290	0.625	0.960	1.31
	Derivative skewness	0.27	1.69	14.6	15.4	14.1
	Number of shocks	0	3	354	664	605

values. In contrast, the SNR is 3–5 dB higher in the low-amplitude case. In Fig. 6(a) there is a region where a 5 dB decrease in SNR results in a substantially lower SNR, and we see similar behavior here. While $\mathrm{Sk}\{\partial p/\partial t\}$ from both numerical and measured data agree for the lower case, a 5 dB decrease in SNR results in substantially underestimating the derivative skewness values for the high-amplitude case. Ultimately, although $\mathrm{Sk}\{\partial p/\partial t\}$ is relatively robust to the presence of noise in the signal, high-frequency noise may still significantly alter measured values.

In the earlier discussion of sampling rates, it was suggested that $f_s/f > 100$ in order to calculate accurate derivative skewness values of at least five for sinusoidal signals. The shock content of the propagating noise waveforms provides a test for this recommendation, though this analysis is limited in scope as the noise considered is not representative of all types of noise. There are many algorithms to identify shocks in a waveform (see Ref. 32 for a recent example); here, a shock is identified as a derivative value exceeding 20 waveform derivative standard deviations to include only the largest outliers. The number of shocks matching this criterion within a 6 s waveform is displayed for each of the microphones in Table I. The 0.4 and 2.6 m microphones have essentially no shock content for both cases. However, differences are seen at 5.6 m. For the 200 Pa case in Fig. 12, $\mathrm{Sk}\{\partial p/\partial t\} = 5.05$ and is still increasing. There are shocks present in the waveform, but fewer than at 8.6 and 11.7 m. This helps illustrate that for $\mathrm{Sk}\{\partial p/\partial t\} \geq 5$, significant shocks have formed in this waveform, providing support for a derivative skewness threshold and associated sampling requirements. These conclusions also draw support from the 286 Pa case. Minimal shocks seen at 0.4 and 2.6 m results in derivative skewness values of 0.27 and 1.69, respectively. However, as the number of shocks greatly increases, $\mathrm{Sk}\{\partial p/\partial t\}$ rises accordingly. While these particular cases corroborate the threshold used in sinusoidal analysis, the results are not general and therefore additional research is needed to understand the evolution of derivative skewness values in the context of random noise.

V. CONCLUSIONS

In this paper, quantitative and physical insights into the evolution of the skewness of the first time difference of a nonlinearly evolving pressure waveform, i.e., the derivative skewness, have been obtained using analytical, numerical, and experimental methods. Analytical forms of the changing derivative skewness have been found for the Earnshaw, Fubini, and Fay solutions. The solutions reveal a sharp increase in the derivative skewness near the shock formation distance, a gradual decrease in the sawtooth region, and a more rapid decrease in the old-age region as the waveform unsteepens. Numerical studies confirm these trends and show that the derivative skewness reaches its maximum between the preshock and sawtooth regions. The effects of additive noise and reduced waveform sampling rate have been investigated; both tend to reduce estimated derivative skewness values. In comparing derivative skewness values for random noise with those of sinusoidal signals, noise will reach greater derivative skewness values over a relatively shorter distance.

The investigation has included practical considerations for nonlinear acoustic signal analysis using the derivative skewness. For sinusoids, in order to observe large derivative skewness values that occur as shocks forms, a sampling rate of at least 100 times the fundamental frequency should be used. Larger sampling rates result in more accurate estimates, provided that the measurement bandwidth is commensurate with the greater sampling rate. The recommended minimum scaled sampling rate allows derivative skewness values of at least 5 to be estimated, which is sufficient to serve as an approximate threshold indicating that a shock is present. The preliminary experimental investigation with noise shows that a similar threshold can also indicate shock formation, though more investigation is needed. These recommendations may provide guidelines for future experiments and allow prior experiments to be more quantitatively interpreted.

ACKNOWLEDGMENTS

The authors thank the reviewers and associate editor for many helpful comments and questions that improved the quality and completeness of the manuscript. This work was funded in part by a grant from the Office of Naval Research. B.O.R. was funded through by an appointment to the Student Research Participation Program at the U.S. Air Force Research Laboratory, 711th Human Performance Wing, Human Effectiveness Directorate, Warfighter Interface Division, Battlespace Acoustics Branch administered by the Oak Ridge Institute for Science and Education through an interagency agreement between the U.S. Department of Energy and USAFRL.

APPENDIX A: SKEWNESS OF A FOURIER SERIES

The skewness of a Fourier series can be expressed analytically in terms of a 2π-periodic function $f(t)$ that may be written as

$$f(t) = \sum_{n=1}^{\infty} A_n \cos(nt) + \sum_{n=1}^{\infty} B_n \sin(nt) = \alpha + \xi, \qquad \text{(A1)}$$

where α is the cosine summation and ξ is the sine summation. The skewness may be written in terms of $E[f^3(t)]$ and $E[f^2(t)]$. Due to periodicity, $E[f^3(t)]$ may be written

$$E\left[f^3(t)\right] = \frac{1}{2\pi}\int_0^{2\pi}(\alpha+\xi)^3 dt \tag{A2}$$

$$= \frac{1}{2\pi}\left[\int_0^{2\pi}\alpha^3 dt + 3\int_0^{2\pi}\alpha^2\xi dt + 3\int_0^{2\pi}\alpha\xi^2 dt + \int_0^{2\pi}\xi^3 dt\right]. \tag{A3}$$

Since ξ is an odd function, the second and fourth integrals are identically zero. The first integral is

$$\int_0^{2\pi}\alpha^3 dt = \int_0^{2\pi}\left\{\sum_{n=1}^{\infty}A_n\cos(nt)\right\}^3 dt \tag{A4}$$

$$= \int_0^{2\pi}\sum_{n=1}^{\infty}\sum_{m=1}^{\infty}\sum_{l=1}^{\infty}A_nA_mA_l \times\cos(nt)\cos(mt)\cos(lt)dt, \tag{A5}$$

$$\sum_{n=1}^{\infty}\sum_{m=1}^{\infty}\sum_{l=1}^{\infty}A_nA_mA_l\int_0^{2\pi}\cos(nt)\cos(mt)\cos(lt)dt. \tag{A6}$$

By repeated use of the trigonometric identity

$$\cos(u)\cos(\nu) = \frac{\cos(u+v)}{2} + \frac{\cos(u-v)}{2}, \tag{A7}$$

the integrand in Eq. (A6) becomes

$$\cos(nt)\cos(mt)\cos(lt) = \frac{1}{4}\left[\begin{array}{c}\cos([m+l+n]t)+\cos([m+l-n]t)\\+\cos([m-l+n]t)+\cos([m-l-n]t)\end{array}\right]. \tag{A8}$$

Each term in Eq. (A8) will integrate to zero unless their individual triple indices (m, n, l) combine to zero, in which case, it will integrate to 2π. These conditions include

$$\begin{aligned} m+l+n&=0,\\ m+l-n&=0,\\ m-l+n&=0,\\ m-l-n&=0. \end{aligned} \tag{A9}$$

Since $n, m, l>0$, the first condition in Eq. (A9) never occurs. The remaining three conditions may be written as

$$\begin{aligned} m+l&=n,\\ m+n&=l,\\ l+n&=m. \end{aligned} \tag{A10}$$

These three conditions may be written in the triple summation in terms of a Kronecker delta,

$$\delta_{n,m} = \begin{cases}1 & n=m\\ 0 & n\neq m,\end{cases} \quad \text{as}$$

$$\int_{-\pi}^{\pi}\alpha^3 dt = \frac{\pi}{2}\left[\sum_{n=1}^{\infty}\sum_{m=1}^{\infty}\sum_{l=1}^{\infty}A_nA_mA_l\delta_{m+l,n} + \sum_{n=1}^{\infty}\sum_{m=1}^{\infty}\sum_{l=1}^{\infty}A_nA_mA_l\delta_{n+m,l} + \sum_{n=1}^{\infty}\sum_{m=1}^{\infty}\sum_{l=1}^{\infty}A_nA_mA_l\delta_{l+n,m}\right]. \tag{A11}$$

By rearranging the arbitrary indices n, m, and l, it can be shown that each of the triple summations in Eq. (A11) are equal to each other. Therefore, the first integral of Eq. (A3) may be written

$$\int_{-\pi}^{\pi}\alpha^3 dt = \frac{3\pi}{2}\left[\sum_{n=1}^{\infty}\sum_{m=1}^{\infty}\sum_{l=1}^{\infty}A_nA_mA_l\delta_{n+m,l}\right]. \tag{A12}$$

The third integral of Eq. (A3) may be found using similar logic. This integral is written

$$\int_{-\pi}^{\pi}\alpha\xi^2 dt = \int_{-\pi}^{\pi}\left\{\sum_{n=1}^{\infty}A_n\cos(nt)\right\}\left\{\sum_{m=1}^{\infty}B_m\sin(nt)\right\}^2 dt \tag{A13}$$

$$= \sum_{n=1}^{\infty}\sum_{m=1}^{\infty}\sum_{l=1}^{\infty}A_nB_mB_l\int_{-\pi}^{\pi}\cos(nt) \times\sin(mt)\sin(lt)dt. \tag{A14}$$

Noting that

$$\sin(a)\sin(b) = \frac{1}{2}\left[\cos(a-b)-\cos(a+b)\right],$$

the integrand of Eq. (A14) may be written

$$\frac{1}{4}\left[\begin{array}{c}\cos([n-m+l]t)+\cos([n+m-l]t)\\-\cos([n-m-l]t)-\cos([n+m+l]t)\end{array}\right]. \tag{A15}$$

Applying the same reasoning used in obtaining Eq. (A11),

$$\int_{-\pi}^{\pi}\alpha\xi^2 dt = \frac{\pi}{2}\left[\sum_{n=1}^{\infty}\sum_{m=1}^{\infty}\sum_{l=1}^{\infty}A_nB_mB_l\delta_{l+n,m} + \sum_{n=1}^{\infty}\sum_{m=1}^{\infty}\sum_{l=1}^{\infty}A_nB_mB_l\delta_{n+m,l} - \sum_{n=1}^{\infty}\sum_{m=1}^{\infty}\sum_{l=1}^{\infty}A_nB_mB_l\delta_{m+l,n}\right]. \tag{A16}$$

By rearranging the arbitrary indices, it can be shown that the first and second triple summations are identical. Then, the third integral in Eq. (A3) may be written

$$\int_{-\pi}^{\pi}\alpha\xi^2 dt = \frac{\pi}{2}\left[2\sum_{n=1}^{\infty}\sum_{m=1}^{\infty}\sum_{l=1}^{\infty}A_nB_mB_l\delta_{n+m,l} - \sum_{n=1}^{\infty}\sum_{m=1}^{\infty}\sum_{l=1}^{\infty}A_nB_mB_l\delta_{m+l,n}\right]. \tag{A17}$$

Thus the expectation value of $f^3(t)$ is

$$E[f^3(t)] = \frac{3}{4}\left[\sum_{n=1}^{\infty}\sum_{m=1}^{\infty}\sum_{l=1}^{\infty}A_nA_mA_l\delta_{n+m,l} + 2\sum_{n=1}^{\infty}\sum_{m=1}^{\infty}\sum_{l=1}^{\infty}A_nB_mB_l\delta_{n+m,l} - \sum_{n=1}^{\infty}\sum_{m=1}^{\infty}\sum_{l=1}^{\infty}A_nB_mB_l\delta_{m+l,n}\right]. \quad \text{(A18)}$$

In the special case that $B_n = 0$ for all n, Eq. (A18) reduces to

$$E[f^3(t)] = \frac{3}{4}\sum_{n=1}^{\infty}\sum_{m=1}^{\infty}\sum_{l=1}^{\infty}A_nA_mA_l\delta_{n+m,l}. \quad \text{(A19)}$$

The expectation value of $f^2(t)$ may be found as well. Again, due to periodicity, we may write

$$E[f^2(t)] = \frac{1}{2\pi}\int_{-\pi}^{\pi}(\alpha+\xi)^2dt + \frac{1}{2\pi}\int_{-\pi}^{\pi}(\alpha^2+\xi^2+2\alpha\xi)dt. \quad \text{(A20)}$$

Since $\alpha\xi$ is an odd function, this term integrates to zero. The remaining terms yield

$$E[f^2(t)] = \frac{1}{2\pi}\int_{-\pi}^{\pi}\left[\left\{\sum_{n=1}^{\infty}A_n\cos(nt)\right\}^2 + \left\{\sum_{n=1}^{\infty}B_n\sin(nt)\right\}^2\right]dt \quad \text{(A21)}$$

$$= \frac{1}{2\pi}\int_{-\pi}^{\pi}\sum_{n=1}^{\infty}\sum_{m=1}^{\infty}[A_nA_m\cos(nt)\cos(mt) + B_nB_m\sin(nt)\sin(mt)]dt \quad \text{(A22)}$$

$$= \frac{1}{2\pi}\sum_{n=1}^{\infty}\sum_{m=1}^{\infty}\left\{A_nA_m\int_{-\pi}^{\pi}\cos(nt)\cos(mt)dt + B_nB_m\int_{-\pi}^{\pi}\sin(nt)\sin(mt)dt\right\} \quad \text{(A23)}$$

$$= \frac{1}{2\pi}\sum_{n=1}^{\infty}\sum_{m=1}^{\infty}(A_nA_m + B_nB_m)\delta_{nm}\pi. \quad \text{(A24)}$$

The expectation value may take the form of Eq. (A24) due to the orthogonality of the integrand of Eq. (A23). The expectation value of $f^2(t)$ may then be simplified to

$$E[f^2(t)] = \frac{1}{2}\sum_{n=1}^{\infty}(A_n^2 + B_n^2). \quad \text{(A25)}$$

Again, in the special case that $B_n = 0$ for all n, Eq. (A25) reduces to

$$E[f^2(t)] = \frac{1}{2}\sum_{n=1}^{\infty}A_n^2. \quad \text{(A26)}$$

Using Eq. (A18) and Eq. (A25), we find that the skewness of $f(t)$ is

$$Sk\{f(t)\} = \frac{3}{\sqrt{2}}\frac{\sum_{n=1}^{\infty}\sum_{m=1}^{\infty}\sum_{l=1}^{\infty}(A_nA_mA_l\delta_{n+m,l} + 2A_nB_mB_l\delta_{l+n,m} - A_nB_mB_l\delta_{m+l,n}))}{\left[\sum_n(A_n^2+B_n^2)\right]^{3/2}}. \quad \text{(A27)}$$

In the special case that $B_n = 0$ for all n, the skewness reduces to

$$Sk\{f(t)\} = \frac{3}{\sqrt{2}}\frac{\sum_{n=1}^{\infty}\sum_{m=1}^{\infty}\sum_{l=1}^{\infty}A_nA_mA_l\delta_{n+m,l}}{\left[\sum_n A_n^2\right]^{3/2}}. \quad \text{(A28)}$$

In the general case, Eq. (A27) must be used if a sum includes both sine and cosine terms, as is the case with discrete sampling. However, if the sum involves only cosine terms, such as the derivative of the Fubini and Fay solutions, the simpler Eq. (A28) may be used.

APPENDIX B: DERIVATIVE SKEWNESS OF A DISCRETELY SAMPLED SAWTOOTH

The derivative skewness of a discretely sampled sawtooth wave can be analytically calculated. If the sawtooth of amplitude p_0 is sampled at a rate of $f_s/f = N$, estimating the derivative values using a two-point finite-difference method results in N points within a wavelength. Of these N points, $N-1$ points have a derivative estimate of $\Delta p/\Delta t = -2p_0/N$ and one point has an estimate of $\Delta p/\Delta t = 2p_0(1-1/N)$, which results in a zero-mean process. The expectation value of $(dp/dt)^n$ is then written as

$$E\left[\left(\frac{dp}{dt}\right)^n\right] = \frac{(N-1)\left(-\frac{2p_0}{N}\right)^n + \left(2p_0\left(1-\frac{1}{N}\right)\right)^n}{N}. \quad \text{(B1)}$$

Substitution of Eq. (B1) into the definition of the derivative skewness in Eq. (1) and simplifying gives

$$Sk\left\{\left(\frac{dp}{dt}\right)\right\} = N^{1/2}\frac{(N-1)\left(-\frac{1}{N}\right)^3 + \left(1-\frac{1}{N}\right)^3}{\left\{(N-1)\left(\frac{1}{N}\right)^2 + \left(1-\frac{1}{N}\right)^2\right\}^{3/2}}. \quad \text{(B2)}$$

For $N \gg 1$, this is approximated as $\mathrm{Sk}\{(dp/dt)\} \cong N^{1/2}$. Since a sawtooth gives the lowest possible average negative derivative values and highest possible positive values for an initially sinusoidal signal, this estimate of a discretely sampled sawtooth gives the greatest possible derivative skewness that can be estimated using a sampling rate of $f_s/f = N$.

[1]D. T. Blackstock, "Nonlinear propagation of jet noise," in *Proceedings of the Third Interagency Symposium on University Research in Transportation Noise*, University of Utah, Salt Lake City, UT (1975), pp. 389–397.
[2]C. L. Morfey and G. P. Howell, "Nonlinear propagation of aircraft noise in the atmosphere," AIAA J. **19**, 986–992 (1981).
[3]K. L. Gee, V. W. Sparrow, M. M. James, J. M. Downing, C. M. Hobbs, T. B. Gabrielson, and A. A. Atchley, "The role of nonlinear effects in the propagation of noise from high-power jet aircraft," J. Acoust. Soc. Am. **123**, 4082–4093 (2008).
[4]K. L. Gee, J. M. Downing, M. M. James, R. C. McKinley, R. L. McKinley, T. B. Neilsen, and A. T. Wall, "Nonlinear evolution of noise from a military jet aircraft during ground run-up," AIAA paper No. 2012–2258 (2012).
[5]B. P. Petitjean and D. K. McLaughlin, "Experiments on the nonlinear propagation of noise from supersonic jets," AIAA paper No. 2003–3127 (2003).
[6]B. P. Petitjean, K. Viswanathan, and D. K. McLaughlin, "Acoustic pressure waveforms measured in high speed jet noise experiencing nonlinear propagation," Int. J. Aeroacoust. **5**, 193–215 (2006).
[7]B. Greska and A. Krothapalli, "On the far-field propagation of high-speed jet noise," *Proceedings of NCAD2008*, paper No. NCAD2008–73071 (2008).
[8]W. J. Baars, C. E. Tinney, M. S. Wochner, and M. F. Hamilton, "On cumulative acoustic waveform distortions from high-speed jets," J. Fluid Mech. **749**, 331–366 (2014).
[9]J. E. Ffowcs-Williams, J. Simson, and V. J. Virchis, "'Crackle': An annoying component of jet noise," J. Fluid Mech. **71**, 251–271 (1975).
[10]M. R. Shepherd, K. L. Gee, and A. D. Hanford, "Evolution of statistical properties for a nonlinearly propagating sinusoid," J. Acoust. Soc. Am. **130**, EL8–EL13 (2011).
[11]S. N. Gurbatov and A. N. Malakhov, "Statistical characteristics of random quasi-monochromatic waves in non-linear media," Sov. Phys. Acoust. **23**, 325–329 (1977).
[12]K. L. Gee, T. B. Neilsen, and A. A. Atchley, "Skewness and shock formation in laboratory-scale supersonic jet data," J. Acoust. Soc. Am. **133**, EL491–EL497 (2013).
[13]P. Mora, N. Heeb, J. Kastner, E. J. Gutmark, and K. Kailasanath, "Near and far field pressure skewness and kurtosis in heated supersonic jets from round and chevron nozzles," in *Proceedings of ASME Turbo Expo 2013*, paper No. GT2013-95774 (2013).
[14]S. A. McInerny, K. L. Gee, J. M. Downing, and M. M. James, "Acoustical nonlinearities in aircraft flyover data," AIAA paper No. 2007–3654 (2007).
[15]S. A. McInerny, M. Downing, C. Hobbs, and M. Hannon, "Metrics that characterize nonlinearity in jet noise," AIP Conf. Proc. **838**, 560–563 (2006).
[16]O. V. Rudenko and S. I. Soluyan, *Theoretical Foundations of Nonlinear Acoustics* (Plenum, New York, 1977).
[17]S. N. Gurbatov, A. N. Malakhov, and N. V. Pronchatov-Rubtsov, "Evolution of higher-order spectra of nonlinear random waves," Radiophys. Quantum Electron. **29**, 523–528 (1986).
[18]D. A. Hennessy, "Crop yield skewness under law of the minimum technology," Am. J. Agr. Econ. **91**, 197–208 (2009).
[19]J. Chen, H. Hong, and J. C. Stein, "Forcasting crashes: Trading volume, past returns, and conditional skewness in stock prices," J. Financ. Econ. **61**, 345–381 (2001).
[20]K. R. Sreenivasan and S. Tavoularis, "On the skewness of the temperature derivative in turbulent flows," J. Fluid Mech. **101**, 783–795 (1980).
[21]S. Tavoularis, J. C. Bennett, and S. Corrsin, "Velocity-derivative skewness in small Reynolds number, nearly isotropic turbulence," J. Fluid Mech. **88**, 63–69 (1978).
[22]C. W. Van Atta and R. A. Antonia, "Reynolds number dependence of skewness and flatness factors of turbulent velocity derivatives," Phys. Fluids **23**, 252–257 (1980).
[23]K. L. Gee, V. W. Sparrow, A. A. Atchley, and T. B. Gabrielson, "On the perception of crackle in high-amplitude jet noise," AIAA J. **45**, 593–598 (2007).
[24]S. A. McInerny. "Launch vehicle acoustics. II—Statistics of the time domain data," J. Aircraft **33**, 518–523 (1996).
[25]K. L. Gee, T. B. Neilsen, M. B. Muhlestein, A. T. Wall, J. M. Downing, M. M. James, and R. L. McKinley, "Propagation of crackle-containing jet noise from high-performance engines," Noise Control Eng. J. **64**, 1–12 (2016).
[26]P. Mora, N. Heeb, J. Kastner, E. Gutmark, and K. Kailasanath, "Impact of heat on the pressure skewness and kurtosis in supersonic jets," AIAA J. **52**, 777–787 (2014).
[27]M. B. Muhlestein and K. L. Gee, "Experimental investigation of a characteristic shock formation distance in finite-amplitude noise propagation," POMA **12**, 045002 (2014).
[28]M. B. Muhlestein, K. L. Gee, T. B. Neilsen, and D. C. Thomas, "Evolution of the average steepening factor for nonlinearly propagating waves," J. Acoust. Soc. Am. **137**, 640–650 (2015).
[29]S. Earnshaw, "On the mathematical theory of sound," Trans. R. Soc. London **150**, 133–148 (1860).
[30]E. Fubini, "Anomalie nella propagazione di ande acustiche de grande apiezza" ("Anomalies in acoustic wave propagation of large amplitude"), Alta Frequenza **4**, 530–581 (1935) [English translation: R. T. Beyer, Nonlinear Underwater Sound, 118–177 (1984)].
[31]R. D. Fay, "Plane sound waves of finite amplitude," J. Acoust. Soc. Am. **3**, 222–241 (1931).
[32]W. J. Baars and C. E. Tinney, "Shock-structures in the acoustic field of a Mach 3 jet with crackle," J. Sound Vib. **333**, 2539–2553 (2014).
[33]D. T. Blackstock, M. F. Hamilton, and A. D. Pierce, "Progressive waves in lossless and lossy fluids," in *Nonlinear Acoustics* (1998), Chap. 4, pp. 65–150.
[34]R. O. Cleveland, "Propagation of sonic booms through a real, stratified atmosphere," Ph.D. dissertation, Department of Mechanical Engineering, The University of Texas at Austin, Austin, 1995.
[35]Loubeau, A. Sparrow, V. W. Pater, L. L., and Wright, W. M., "High-frequency measurements of blast wave propagation," J. Acoust. Soc. Am. **120**, EL29–EL35 (2006).
[36]S. A. McInerny and S. M. Olcmen, "High intensity rocket noise: Nonlinear propagation, atmospheric absorption, and characterization," J. Acoust. Soc. Am. **117**, 578–591 (2005).
[37]D. T. Blackstock, "Connection between the Fay and Fubini solutions for plane sound waves of finite amplitude," J. Acoust. Soc. Am. **39**, 1019–1026 (1966).
[38]J. A. Gallagher and D. K. McLaughlin, "Experiments on the nonlinear characteristics of noise propagation from low and moderate Reynolds number supersonic jets," in *7th Aeroacoustics Conference* (1981), pp. 1981–2041.
[39]S. N. Gurbatov and O. V. Rudenko, "Statistical phenomena," in *Nonlinear Acoustics*, edited by M. F. Hamilton and D. T. Blackstock (Academic Press, San Diego, 1998), Chap. 13, pp. 377–398.
[40]F. M. Pestorius and D. T. Blackstock, "Propagation of finite-amplitude noise," in *proceedings of Finite-Amplitude Wave Effects in Fluids*, Copenhagen (1973), pp. 24–29.
[41]M. B. Muhlestein and K. L. Gee, "Evolution of the temporal slope density function for waves propagating according to the inviscid Burgers equation," J. Acoust. Soc. Am. **139**(2), 958–967 (2016).